Přírodovědecká fakulta
Faculty of Science

Jihočeská univerzita v Českých Budějovicích
University of South Bohemia in České Budějovice

Bachelor Thesis

Characterization of *Trypanosoma brucei* MICOS subunit Mic20.

Sebastian Deisenhammer

Supervised by doc. Hassan Hashimi, Ph.D.
Co-supervised by RNDr. Jiri Heller
Laboratory of Molecular Biology of Protists
Institute of Parasitology, Biology Centre, Czech Academy of Sciences

České Budějovice 2021

Deisenhammer S., 2021: Characterization of *Trypanosoma brucei* MICOS subunit Mic20. Bc. Thesis in English – 38 p., Faculty of Science, University of South Bohemia, České Budějovice, Czech Republic.

Annotation

This study focuses on the trypanosome MICOS complex related membrane protein Tb927.10.11900 (TbMic20) in *Trypanosoma brucei*. This research aimed to express TbMic20 in *E. coli* cells under soluble conditions and further determine its standard redox potential.

Declaration

I hereby declare that I have worked on my bachelor's thesis independently and used only the sources listed in the bibliography. I hereby declare that, in accordance with Article 47b of Act No. 111/1998 in the valid wording, I agree with the publication of my bachelor thesis, in full to be kept in the Faculty of Science archive, in electronic form in publicly accessible part of the STAG database operated by the University of South Bohemia in České Budějovice accessible through its web pages.
Further, I agree to the electronic publication of the comments of my supervisor and thesis opponents and the record of the proceedings and results of the thesis defence in accordance with aforementioned Act No. 111/1998. I also agree to the comparison of the text of my thesis with the Theses.cz thesis database operated by the National Registry of University Theses and a plagiarism detection system.

České Budějovice …… ……

Sebastian Deisenhammer

Acknowledgements

First, I would like to express my gratitude to my supervisor, doc. Hassan Hashimi, PhD, for accepting me to work as part of his team and sharing his knowledge with me. Thank you for the time you spent discussing results and researching for the experiments. Next, I would like to thank my co-supervisor, RNDr. Jiri Heller who always guided me through new experiments and was always kind and helpful. Thank you so much for your support throughout my stay in your laboratory.

Moreover, I want to thank the whole team of the Lab of Functional Biology of Protists, especially Iosef Kaurov, for providing me with the knowledge to complete this thesis.

Table of content

Abbreviations

A adenine

AA amino acid

Asn asparagin

ATP adenosine triphosphate

bp base pairs

CL cell lysate

CJ cristae junction

Cys/C Cysteine

DNA deoxyribonucleic acid

dNTP deoxyribose nucleoside triphosphate

FT flow through

G guanine

Glu glutamic acid

Gln glutamine

GSH reduced glutathione

GSSG oxidized glutathione

Gly glycine

IMS intermembrane space

IPTG isopropyl β-D-1 -thiogalactopyranoside

kDNA kinetoplast DNA

LB lysogeny broth

LD loading dye

LDS lithium dodecyl sulfate

MIA mitochondrial intermembrane space assembly

MICOS mitochondrial contact site and cristae organization system

MIM mitochondrial inner membrane

MOM mitochondrial inner membrane

Ni-NTA nickel-nitrilotriacetic acid

OD600 optical density at 600 nm

PBS phosphate-buffered saline

PAGE polyacrylamide gel electrophoresis

PCR polymerase chain reaction

Phe Phenylalanine

PVDF polyvinylidene fluoride

RNAi RNA interference

rpm revolutions per minute

rProtein recombinant protein

RT room temperature

SAM sorting assembly machinery

SDS sodium dodecyl sulfate

T thymine

Tyr tyrosine

TOM translocase of the outer membrane

1. Introduction

1.1 Trypanosoma brucei

Trypanosoma brucei is a eukaryotic unicellular parasite belonging to the Kinetoplastids (Eukaryota, Excavata, Euglenozoa), a group of flagellated protozoans (Stuart et al., 2008). The mitochondrial DNA of the Kinetoplastids is condensed into a massive body called kinetoplast (kDNA), which is specific to the taxonomic group (Simpson et al., 2002). *Trypanosoma brucei* is spread through the bite of the tsetse fly and causes the human African trypanosomiasis, also known as African sleeping sickness. Through its life cycle, *Trypanosoma brucei* has different stages in its hosts, in which it has different internal organization and cell shapes: The procyclic and the bloodstream form (Höög et al., 2010; Matthews et al., 2004).

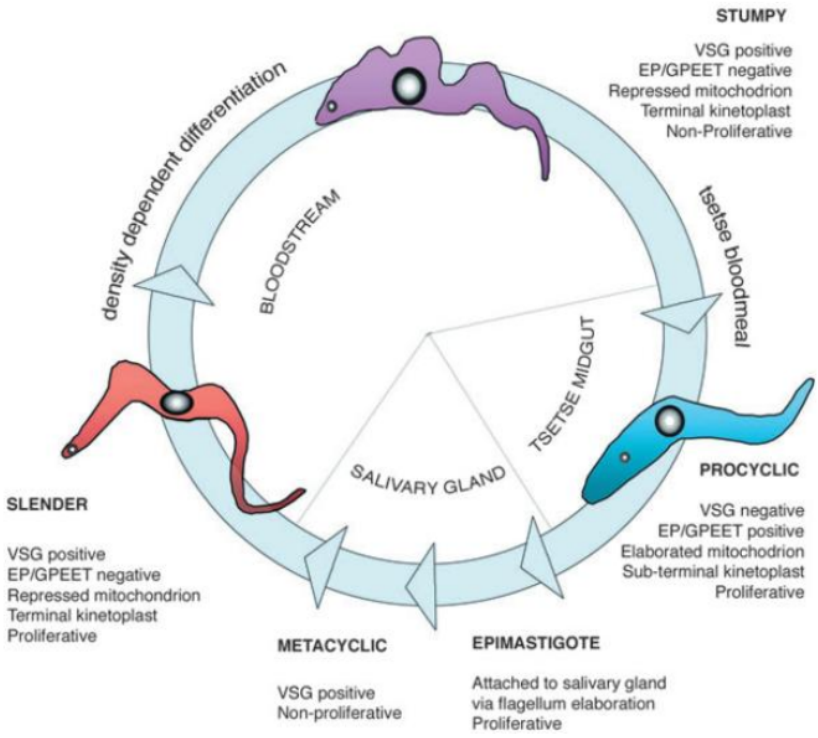

Figure 1: ***Schematic life cycle of Trypanosoma brucei;*** *taken from Matthews, 2005.*

The cell biological processes and organization of the cell structure are fundamental to all cells. Trypanosome brucei must adapt to different environments in the tsetse fly and mammalian hosts to escape the immune response of the organisms (Matthews, 2005). The procyclic form is found

inside the tsetse fly midgut, whereas the bloodstream form occurs in humans and cattle, depending on the subspecies (Höög et al., 2010). Due to the fact that the subspecies *Trypanosoma brucei brucei* is not human infective and the two life cycle forms are easily kept in vitro, it has become a model organism of the protozoan order of the Kinetoplastida for investigation of the evolution of fundamental molecular and cellular biology of eukaryotes (Brun et al., 2010; Matthews, 2005)

1.2 The Mitochondrial contact site and Cristae Organization System

Mitochondria are eukaryotic organelles, commonly called the 'powerhouse' of the cell, and the site of ATP synthesis through oxidative phosphorylation and numerous other essential functions (Roger et al., 2017). Originating from an endosymbiotic α-proteobacterium, mitochondria are enveloped in the mitochondrial outer membrane (MOM) and mitochondrial inner membrane (MIM), with the mitochondrial matrix inside and the intermembrane space (IMS) between the two membranes (Muñoz-Gómez et al., 2015).

Through the narrow neck-like structures Cristae junction (CJs), where the MIM is sharply bent, the MIM can further be divided into the inner boundary membrane, neighbouring the MOM, and cristae membranes, where the respiration chain complexes, and ATP synthase are predominately incorporated. These invaginations increase the overall surface of the MIM and allow high concentrations of integral membrane proteins (Barbot & Meinecke, 2016; Davies et al., 2011; Gilkerson et al., 2003).

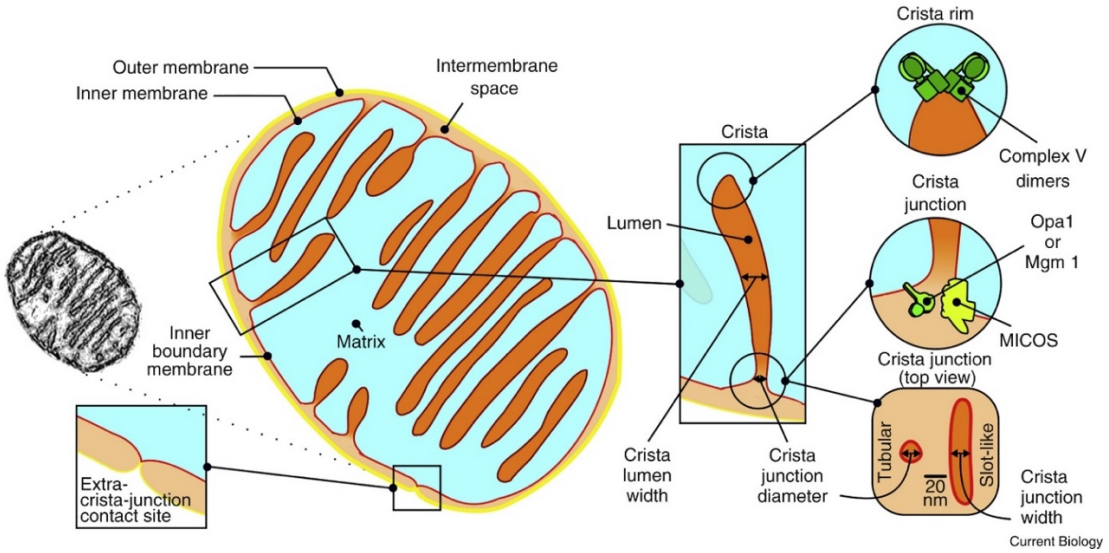

Figure 2: ***Typical architecture of a mitochondrion*** *based on a three-dimensional reconstructed mitochondrion. Taken from Pánek et al., 2020.*

A multiprotein complex called the Mitochondrial contact site and Cristae Organization System (MICOS) is responsible for the maintenance and organization of cristae formation, which appears to be conserved in all mitochondria capable of oxidative phosphorylation (Harner et al., 2011).

As core subunits for membrane bending in yeast, Mic10 and Mic60 were identified as depletion of the proteins lead to loss of CJs and formation of abnormal cristae (Barbot et al., 2015; Bohnert et al., 2015; Friedman et al., 2015; Guarani et al., 2015). In contrast to yeast, the trypanosome MICOS complex has two Mic10 subunits localizing to cristae membranes and Mic60 lacking the sorting assembly machinery (SAM50) interaction mediating mitofilin domain (Huynen et al., 2016; Muñoz-Gómez et al., 2015). Despite the lack of this domain, the interaction of TbMICOS and TbSAM50 was confirmed (Kaurov et al., 2018). Upon RNAi silencing of TbMic20, one of the other five TbMICOS subunits, downregulation of the Mitochondrial FAD-linked sulfhydryl oxidase (TbERV1) in the IMS occurred (Kaurov et al., 2018). In most anaerobic eukaryotes, ERV1 is linked to the oxidoreductase pathway of Mia40 (Edwards et al., 2020; Mordas & Tokatlidis, 2015). The effect of the downregulation of TbMic20 on TbERV1 therefore suggests a role of TbMic20 in oxidative folding (Kaurov et al., 2018).

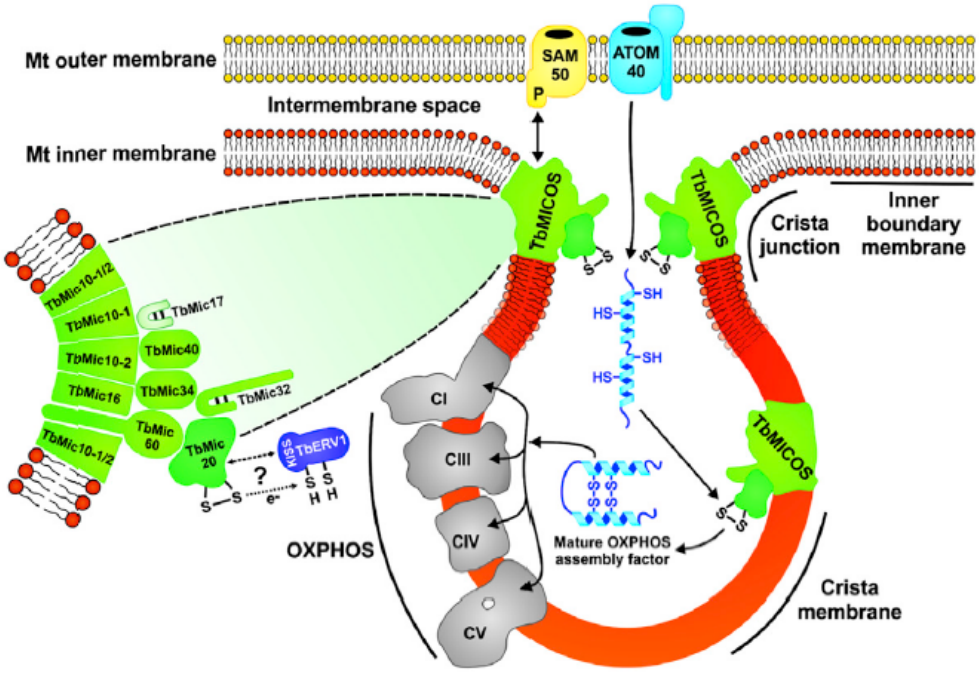

Figure 3: ***Proposed role of TbMICOS.*** *Showcased is a theoretical composition of the MICOS subunits (green) and the predicted role of TbMic20 in oxidative folding of IMS proteins (blue). Taken from Kaurov, 2018.*

1.3 The Mitochondrial IMS Assembly (MIA) Pathway

Since mitochondria depend on the correct import and targeting of proteins synthesized in the cytosol, different protein machinery are responsible for the further process. One of these machinery is Mia40, which is an oxidoreductase responsible for oxidative folding of proteins containing cysteine residues (Mordas & Tokatlidis, 2015; Stojanovski et al., 2012). Oxidative folding describes the generation of the native disulfide bonds of a protein-based on oxidation, reduction, and reshuffling (Narayan et al., 2000)

Located in the IMS, Mia40 catalyzes the formation of disulfide bonds between cysteine residues, which is vital for the structural stability of proteins and further involvement in redox pathways (Banci et al., 2009; Koch & Schmid, 2014). The translocase of the outer membrane (TOM) is the import gate of mitochondrial proteins into the IMS and, therefore also the start of the MIA pathway (Böttinger et al., 2012; Dolezal et al., 2006). Imported proteins containing specific cysteine rich motifs (CX_3C, CX_9C) are recognized and captured by Mia40 (Milenkovic et al., 2007).

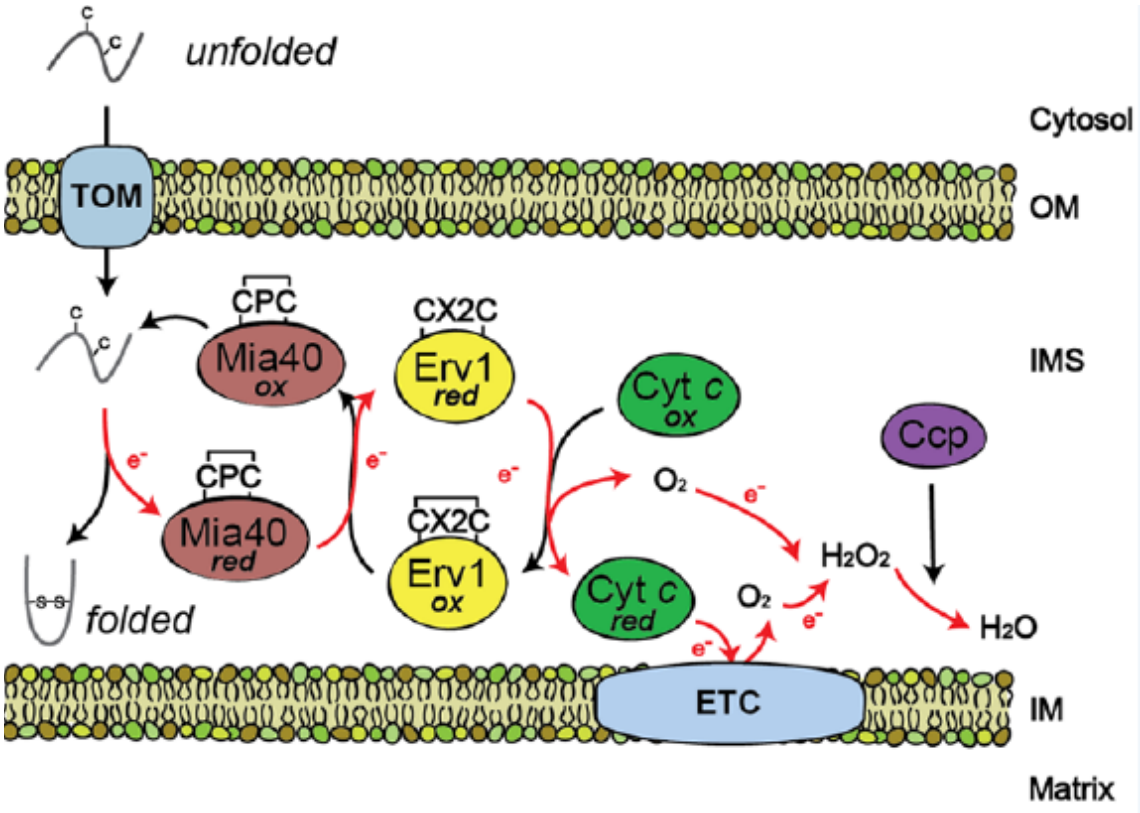

Figure 4: ***Scheme of the electron transfer across the MIA pathway.*** *Taken from Mordas and Tokatlidis, 2015.4*

The characteristic dithiol/disulfide active Cysteine-Proline-Cysteine (CPC) motif introduces disulfide bonds to the precursor proteins by oxidation (Figure 1) and Mia40 is thereby reduced (Chacinska et al., 2004). ERV1 accepts the transferred electrons, which leads to the regeneration through oxidation of Mia40 and the reduction of ERV1. Lastly, ERV1 is oxidized by renewed electron transfer to cytochrome c or oxygen, which ultimately connects Mia40 to the respiratory chain (Banci et al., 2009; Chatzi et al., 2013; Mordas & Tokatlidis, 2015).

Interestingly, by use of comparative genomics, studies showed that *T. brucei* does not possess Mia40, and an alternative mechanism to the MIA pathway remained unidentified. (Allen et al., 2008; Haindrich et al., 2017). However, previous work predicted TbMic20 to have a thioredoxin-like structure and a Cysteine-Isoleucine-Proline-Cysteine (CIPC) motif, similar to the CPC motif of MIA40. It, therefore, gained attention as a possible functional analogue as the central MIA enzyme in opisthokonts (Kaurov et al., 2018; Wideman & Muñoz-Gómez, 2018). This thesis aims to strengthen this assumption by determination of the standard redox potential of TbMic20.

2. Aims of the Thesis

The first aim of this thesis was to optimize the expression of the protein TbMic20 of *Trypanosoma brucei* in *Escherichia coli* (*E. coli)* cells to increase the solubility of the protein. Verifications were made using several molecular biological techniques such as SDS-PAGE and western blot analysis, and affinity chromatography. To determine the redox potential of the protein, fluorescence measurements using reduced and oxidized glutathione were performed. For further examination of the protein, the characteristic CIPC motif of the protein was changed by site-directed mutagenesis.

3. Material and Methods

3.1 Cell constructs

To express and analyze TbMic20, a pSKB-3 plasmid (Addgene plasmid # 62540 ; http://n2t.net/addgene:62540 ; RRID:Addgene_62540) containing a polyhistidine-tagged TbMic20 was generated and transformed to *Escherichia Coli* BL21-strain. These constructs were generated before my work on this thesis by RNDr. Jiri Heller.

3.1.1 Cell cultivation

To maintain the liquid cell culture, the culture containing the cell constructs was regrown before experiments or at least once a month. For regrowing the liquid culture, 8 µL of kanamycin (30 µg/µL) was added to 5 mL of LB media (Table 1.). 50 µL of cell culture were added to the LB media and incubated overnight in an incubating shaker (Lab Companion Incubating Shaker) at 37°C and 200 RPM. The cell culture was then stored at 5°C.

Table 1: LB Media

reagent	*concentration*
Tryptone	10 g/L
NaCl	10 g/L
Yeast Extract	5 g/L

3.2 Determination of expression conditions for rMic20 in E. coli

3.2.1 Expression of rMic20 in E. coli

Prior to the expression of the protein, a new culture was regrown (according to section 3.1). After the overnight incubation, 0.5 ml of the cell culture was added to 10 ml of LB media (Table 1.) and put into an incubating shaker. The optical density was measured with an Eppendorf BioPhotometer, and incubation is stopped when the OD600 reached a value of 0.6. To induce the expression, Isopropyl-β-D-thiogalactopyranoside (IPTG) was added to a final concentration of 1 mM. The culture was then put to an incubating shaker (Innova 44 Incubating Shaker) under the different conditions described in Table 2.

Table 2: Conditions for expression of the recombinant protein

Temperature:	***Duration:***
37 °C	1 hour
25 °C	14 hours
20 °C	14 hours
14 °C	16 hours

3.2.2 Extraction of soluble and insoluble fractions of Mic20

For the determination of the amount of the soluble cell fraction, the cell culture was harvested by centrifugation at 4000 rpm at 4 °C for 20 minutes. The supernatant was discarded, and the cells were resuspended in 1 ml of 1x phosphate-buffered saline (PBS). In order to lyse the cell walls, the culture was frozen in liquid nitrogen and thawed on ice. Further, an ultrasonic homogenizer (BioLogic Inc. Ultrasonic Homogenizer Model 3000) was used to sonicate the cells six times for 10 seconds with 10 seconds pause at 50% power and 50% pulse. The lysate was centrifuged at 10,000 rpm at 4°C for 20 minutes to separate soluble and insoluble fractions. The supernatant containing the soluble fraction was decanted and saved on ice. For suspension of the insoluble matter, the pellet was resuspended in 1 mL of 1x PBS and 10 µL of Triton X-100. To address the amount of insoluble and soluble fraction of rMic20, SDS-PAGE was performed for visualization of the protein fractions.

3.2.3 SDS-PAGE analysis

For this purpose, 30 µL of each sample was mixed with 10 µL of 4X lithium dodecyl sulfate loading buffer (NuPAGE™ LDS Sample Buffer 4X) and boiled at 95 °C for 5 minutes. For analysis, Bolt™ 4-12% Bis-Tris Plus (SDS) gel (Invitrogen) was covered with 250 ml of running buffer consisting of 12.5 mL 20X Bolt™ MOPS SDS Running buffer (ThermoScientific) and 237.5 mL MilliQ H_2O. Prior to the loading of the samples, the wells of the polyacrylamide gel were washed by gently pipetting MOPS running buffer into the well. Then 20 µL of the sample were loaded, and the electrophoresis was performed at 125 V for approximately 1.5 hours.

3.2.4 Western blot analysis

Prior to the western blot analysis, a piece of polyvinylidene difluoride (PVDF) blotting membrane (GE Healthcare Life Science) with the dimension of 8 cm x 7.5 cm was prepared, and the PVDF membrane was submerged in methanol for 10 minutes. Additionally, two filter papers with the dimension of 8.5 cm x 8 cm were submerged in pre-cooled transfer buffer.

Next, the gel and the activated PVDF membrane were arranged in the following order: sponge – filter paper – gel – PVDF membrane – filter paper – sponge. During the arrangement, it was ensured that no air bubbles were trapped inside the layers and then transferred to the transfer apparatus. The apparatus was filled with transfer buffer and transferred at 100 V for at least 1.5 hours. After the transfer, the PVDF membrane was blocked overnight at 4°C in a blocking solution containing PBS-T (1X PBS + 1% (v/v) Tween 20)) and 4% (w/v) powdered milk. After blocking, the membrane was transferred to a 50 mL falcon tube and incubated with a primary antibody (Anti-HA, Thermo Scientific), diluted in blocking solution in a 1:1000 ratio for at least 1 hour under constant rotation. The solution was discarded, and the membrane was washed three times with 1x PBS-T for 10 minutes under rotation.

Next, the membrane was incubated with a secondary antibody (Anti-mouse) diluted in blocking solution in a 1:1000 ratio for at least 1 hour under constant rotation. After incubation with the second antibody, the washing with 1x PBS-T for 10 minutes under rotation was again repeated three times.

Clarity Western ECL Substrate (BioRad) was used for visualization of the proteins. For this purpose, 200 µL of Clarity Western Peroxide Reagent and 200 µL of Clarity Western Luminol/Enhancer Reagent were mixed and spread upon the PVDF-membrane. A ChemiDoc™ MP imaging system was used for performing the chemiluminescent detection and visualized with BioRad Image Lab software.

3.3 Purification of rMic20

3.3.1 Affinity chromatography

Affinity chromatography was performed to isolate the protein. For this purpose, rMic20 expression prior to the day of purification was performed. To increase the amount of isolated protein, the amount of freshly regrown culture was increased to 10 mL and the LB-media (Table

1) to 200 mL. The expression was then performed according to section 3.2.1 at 20°C for 14 hours.

After the expression, the cell culture was harvested by centrifugation at 4000 rpm at 4°C for 10 minutes. The supernatant was discarded, and the pellet was resuspended in 10 ml Lysis buffer (Table 3). Then the suspension was sonicated with an ultrasonic homogenizer (BioLogic Inc. Ultrasonic Homogenizer Model 3000) six times for 10 seconds with 10 seconds pause at 50% power and 50% pulse. Next, centrifuge at 4000 rpm and 4°C for 10 minutes and collect the supernatant. For the purification, a stand holder with a BioRad Poly Prep Chromatography Column was set up. 750 µL of Novex™ Ni-NTA Agarose (Invitrogen™) were transferred to the column and mixed well.

The beads were resuspended in 1 mL of lysis buffer for washing, and the buffer is flowed through. 10 mL of cell lysate were transferred to the chromatography column and put to a MultiBio RS-24 rotator at 4° for 1 hour to enable the his-tagged protein to bind to the beads. After binding, the column is reinserted into the stand, and the flow-through is collected and labelled "FT". For the washing steps, 4 mL of washing buffer (Table 4) are transferred to the column, and the flow-through is collected. The washing step was repeated three times, and the samples were properly labelled "W_1, W_2, W_3". The elution steps were performed by transferring 0.5 mL of elution buffer (Table 5) to the column, and the buffer was flown through and collected. This step was performed three times, and the samples were labelled "E_1, E_2, E_3". The samples were subsequently analyzed by SDS-PAGE according to section 3.2.3, followed by G250 Coomassie blue staining.

Table 3.: Lysis Buffer

reagent	*molarity*	*concentration*
$NaH_2PO_4 \cdot 2H_2O$	50 mM	7.8 g/L
NaCl	300 mM	17.54 g/L
Imidazole	10 mM	0.68 g/L
		Adjust pH to 8.0 by adding 3 M NaOH

Table 4.: Wash Buffer

reagent	*molarity*	*concentration*
$NaH_2PO_4 \cdot 2H_2O$	50 mM	7.8 g/L
NaCl	300 mM	17.54 g/L
Imidazole	20 mM	1.36 g/L
		Adjust pH to 8.0 by adding 3 M NaOH

Table 5.: Elution Buffer

reagent	*molarity*	*concentration*
$NaH_2PO_4 \cdot 2H_2O$	50 mM	7.8 g/L
NaCl	300 mM	17.54 g/L
Imidazole	250 mM	17.0 g/L
	Add ½ cOmplete EDTA-free Protease Inhibitor Tablet per litre	
	Adjust pH to 8.0 by adding 3 M NaOH	

3.3.2 Coomassie Blue staining

In order to visualize the gel after SDS-PAGE, the gel was gently washed with MilliQ H_2O and stained for 1 hour in a staining solution containing 0.1% Coomassie Brilliant Blue R-250, 50% methanol and 10% acetic acid. The gel was again washed with MilliQ H_2O to remove the excess of the staining solution. For distaining of the gel and visualizing the protein bands, the gel was incubated in 7% acetic acid for at least 1 hour. The gel was then digitalized using a ChemiDoc™ MP imaging system and BioRad Image Lab software.

3.3.3 Cleavage of poly histidine-tag on the recombinant protein

AcTEV™ Protease (Invitrogen) was used to remove the poly histidine-tag of the recombinant protein. AcTEV™ Protease enables the removal of the poly histidine-tag by recognition of a seven amino acid sequence (Glu-Asn-Leu-Tyr-Phe-Gln-Gly). First, the concentration of the protein was measured with a NanoDrop™ 1000 Spectrophotometer (Thermo Scientific) by measuring absorbance at 260 nm (A_{260}). To increase the obtained recombinant protein without poly histidine-tag, approximately 400 µg of the purified protein were used for the reaction to a total volume of 190 µl (Table 6) in an Eppendorf tube and left for 2 hours at room temperature. The protein was then purified by affinity chromatography and verified by SDS-PAGE according to sections 3.2.3 & 3.3.2, and the concentration was measured.

Table 6. AcTEV Protease reaction.

reagent	*volume*
rProtein (2.9µg/µL)	150 µl (435µg)
20X TEV Buffer (Invitrogen)	9.5 µl
AcTEV™ Protease (Invitrogen)	21.75 µl
MilliQ H_2O	8.25 µl

3.4 Assessing the redox potential of rMic20

3.4.1 Fluorescence Spectroscopy

To determine if rMic20 reacts to reducing and oxidizing conditions, an excitation scan was performed to determine the emission wavelength for the following fluorescence measurements. This procedure is based on previous work on thioredoxin-like proteins, due to the thioredoxin-like structure of TbMic20 (Haugstetter et al., 2005). For this purpose, rMic20 was expressed and purified according to section 3.3 and mixtures containing a final concentration of 5 µM of the purified protein and 0.1 mM of oxidized glutathione (GSSG) and varying concentrations of reduced (GSH) glutathione in 50 mM phosphate buffer (Table 7.) were prepared.

The phosphate buffer was degassed and flushed with N_2 with the use of a homemade degassing station of the anaerobic and molecular microbiology lab (https://soilwater.eu/people/petras-daniel/). Reaction mixtures were prepared to a final volume of 500 µL and following concentrations of either 0.1mM GSSG and varying concentrations of GSH. The mixtures were incubated for 16 hours in an anaerobic chamber (Oxoid™ AnaeroJar™, ThermoFisher) Scientific and then loaded on a Nunc™ Micro Well™ 96-Well flat-bottom microplate. The emission scan was performed on a TECAN Spark® multimode-microplate-reader and the SparkControl application with a method according to Table 8.

Table 7. 100 mM Phosphate Buffer

Component	***amount***
$Na_2HPO_4 \cdot 12H_2O$	20.701 g
$NaH_2PO_4 \cdot 2H_2O$	6.584 g
MilliQ H_2O	to 1 L
	adjust pH to 7.0 with HCl or NaOH

Table 8. Excitation Scan Method

Setting	***Value***
Mode	Fluorescence Intensity Scan Top Reading
Excitation	Monochromator
Excitation Wavelength	280 nm
Emission wavelength - start	305 nm
Emission wavelength - end	400 nm
Emission wavelength step size	1 nm
Gain	40

3.4.2 Redox Equilibrium of rMic20 and Glutathione

After the excitation at 280 nm and 295 nm, the wavelength at which the maximal difference in fluorescence intensity of oxidized and reduced protein was observed was determined at 333 nm. Fluorescence Intensity measurements were taken based on previous work on thioredoxin-like proteins (Haugstetter et al., 2005; Loferer et al., 1995). For this purpose, samples were prepared according to section 3.4.1 with a final concentration of both 0.1 mM GSSG and GSH in a range from 0.01 mM to 20 mM. The method of the procedure was according to Table 9. The redox equilibrium of rMic20 with glutathione is given by Equation 1. The relative amount of reduced rMic20 (R) at equilibrium was calculated using Equation 2 and plotted against the $[GSH]^2/[GSSG]$ ratio. The combination of Equation 2 and Equation 3 leads to Equation 4, and linear transformation of this graph and fitting the data to equation 3 were used to determine the equilibrium constant K_{eq} (Hawkins et al., 1991). Graphical representation was performed using OriginPro software (www.originlab.com) using the license of the Johannes Kepler University Linz. Determination of the standard redox potential of the recombinant protein was calculated by use of the Nernst Equation (Equation 5) at pH 7.0, 298.15 K and using the standard potential of glutathione of -0,240 V (Müller, 2019).

$$TbMic20^{SH} + GSSG \rightleftarrows TbMic20^{SS} + 2\,GSH \quad (Eq.1)$$

$$R = {(F - F_{ox})}\Big/{(F_{red} - F_{ox})} \quad (Eq.2)$$

$$R = {[GSH]^2/[GSSG]}\Big/{K_{eq} + [GSH]^2/[GSSG]} \quad (Eq.3)$$

$$F = \frac{[GSH]^2/[GSSG] \times (F_{red} - F_{ox})}{K_{eq} + [GSH]^2/[GSSG]} + F_{ox} \quad (Eq.4)$$

$$E_0 = E_{0(GSH/GSSG)} - \frac{RT}{nF} \times \ln(K_{eq}) \quad (Eq.5)$$

F…..... measured fluorescence intensity

F_{red}….. Fluorescence intensity of reduced protein

F_{ox}……Fluorescence intensity of oxidized protein

Table 9. Intensity scan method

Setting	*Value*
Mode	Fluorescence Intensity Scan Top Reading
Excitation	Monochromator
Excitation Wavelength	280 nm
Excitation bandwidth	20 nm
Emission wavelength	333 nm
Gain	40
Temperature	25°C

3.5 C80 and C83 rMic20 Mutants by Mutagenesis

3.5.1 DNA Isolation

The plasmid of the liquid cell culture was extracted using a DNA purification kit (GeneAll®Hybrid-Q™ Plasmid Rapidprep) following the Standard Hybrid-Q™ Standard protocol. For this purpose, a fresh cell culture was prepared according to section 3.1.1. The DNA extraction was verified using gel electrophoresis with a GeneRuler 1kb plus DNA ladder as size standard (Figure 5).

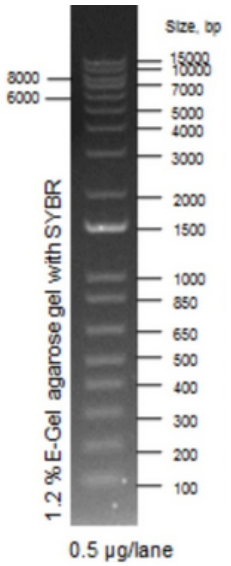

Figure 5: ***GeneRuler 1 kb plus DNA ladder*** *(Taken from Thermo Fisher* Scientific).

3.5.2 Gel electrophoresis

PCR products and DNA fragments from restriction digestion were verified using gel electrophoresis. For this purpose, a 1 % agarose gel in 1x TAE electrophoresis buffer (Table 7) with 3 µL of 10 mg/ml ethidium bromide per 80 ml of melted agarose was prepared. After the gel has solidified, 2 µl of DNA loading dye was added to 10 µl of DNA sample and loaded on the agarose gel. For size reference, 10 µl of GeneRuler 1kb Plus DNA ladder (Thermo Scientific) were loaded onto the gel. The electrophoresis was performed at 110 V for 30 to 45 minutes, and the bands were visualized under UV-light using a ChemiDoc™ MP imaging system and BioRad Image Lab software.

Table 10: ***10X TAE electrophoresis Buffer***

reagent	***concentration***
tris	40 mM
Acetic acid	200 mM
ethylenediaminetetraacetic acid (EDTA), pH 8.3	10 mM
MilliQ H_2O	

3.5.3 Site-directed mutagenesis

Site-directed mutagenesis was used to exchange the cysteine of the CIPC motif on positions 80 and 83 with serin. Site-directed mutagenesis, a polymerase chain reaction (PCR) based method, requires a primer, where one a base of interest is exchanged. By use of PCR, the primer still hybridizes with the DNA and the mutation is incorporated in the product. For this purpose, primers on Table 8 were designed to exchange TGC (Cysteine) to AGC (Serin). The mutagenesis was performed with a BioRad C1000™ Thermal cycler and a program according to Table 9 and reaction mixture according to table 10.

The products were verified by gel electrophoresis according to section 3.5.2. To extract the mutagenesis product, a gel purification was performed with a GenElute™ Gel Extraction Kit (Sigma-Aldrich Co. LLC) according to the manufacturer's protocol. The linear DNA was then reconnected using T4-DNA Ligase (Roche, Sigma-Aldrich Co. LLC) with a reaction mixture according to Table 11. For 3 hours at room temperature and again verified by gel electrophoresis according to section 3.5.2.

Table 11: ***Primer sequences; changed nucleotides in bold.***

Mutation	***Primer***	***Sequence***
C80S rMic20	Forward	GAAGCACGGAA**AGC**ATCCCGTGCC
C80S rMic20	Reverse	CAGTACTTAACCACCATAATTTCGTCTTTGTG
C83S rMic20	Forward	ATGCATCCCG**AGC**CTCTCATTGG
C83S rMic20	Reverse	CCGTGCTTCCAGTACTTAAC

Table 12: ***Thermal cycler program***

step	*temperature*	*time*
Initial denaturation	98°C	30 seconds
25 Cycles	98°C	5–10 seconds
	63°C	10–30 seconds
	72°C	120 seconds
Final Extension	72°C	2 minutes
Hold	4°C	

Table 13: ***Site-directed mutagenesis reaction mixture***

Component	*Volume*
Q5 High-Fidelity 2X Master Mix	25 µl
10 µM Forward Primer	2.5 µl
10 µM Reverse Primer	2.5 µl
Template DNA	1-10 ng
MilliQ H_2O	to 50 µl

Table 14: ***T4-DNA-Ligase reaction mixture***

Component	*Volume*
Mutagenesis Product [39ng / µL]	1 µL
T4-DNA-Ligase	2.5 µL
10X T4 DAN-Ligase Buffer	3 µL
MilliQ H_2O	23.5 µL

3.5.4 Transformation into XL1-Blue competent cells

The DNA products were transformed into XL1-Blue competent *E. coli* cells by heat shock. Prior to the transformation, LB agar plates were made by the addition of 7.5 g agar to 500 mL of LB broth (Table 1). In order to enable positive selection for bacteria containing a pSKB-3 plasmid, kanamycin (100 µg/mL) was added. For this purpose, 10 µL of plasmid DNA were

incubated with 50 µL of host cells on ice for 30 minutes in an Eppendorf tube. Then the tube was transferred to a water bath at 42°C for exactly 60 seconds, followed by incubation on ice for 5 minutes. Next, 400 µL of pre-warmed (37°C) super optimal broth (SOC) medium (Table 12) was added and put in an incubating shaker (Lab Companion Incubating Shaker) at 37°C and 200 RPM for 1 hour. The mixture was then spread on a pre-warmed (37°C) agar plate and incubated at 37°C overnight. Then 4 colonies of each mutant were collected with sterile toothpicks and incubated in 5ml LB media with 8 µL of kanamycin (30 µg/µL) in an incubating shaker (Lab Companion Incubating Shaker) at 37°C and 200 RPM overnight. To verify the constructs, the plasmid DNA was isolated according to 3.5.1 and a restriction digest using CutSmart® Buffer (NEB) and the restriction enzymes BamH I and Hind III with a reaction mixture according to table 13 for 30 minutes at room temperature was performed. However, the DNA isolation failed for unknown reasons. RNDr. Jiri Heller repeated the isolation and restriction digestion. He verified the restriction by gel electrophoresis and isolated the gene of interest using a GenElute™ Gel Extraction Kit (Sigma-Aldrich Co. LLC) according to the manufacturer's protocol. By sending the DNA for sequencing to Eurofins Scientific, he was able to confirm the creation of the C80 and C83 mutants.

Table 15: ***SOC medium.***

component	***Final concentration***
yeast extract	0.5%
tryptone	2 %
NaCl	10 mM
KCl	2.5 mM
$MgSO_4 \cdot 7H_2O$	10 mM
$MgCl_2 \cdot 6H_2O$	10 mM
Glucose	20 mM
MilliQ H_2O	

Table 16: ***Restriction digestion reaction.***

reagent	***volume***
BamH I (NEB)	1 µl
Hind III (NEB)	1 µl
CutSmart® Buffer 10X (NEB)	2 µl
rMic20 DNA	1 µl
Milli Q H_2O	15 µl

4. Results

4.1 Expression and extraction of rMic20 in E. coli

To address the solubility of rMic20, the recombinant protein was expressed in *E. coli*.
The protein sequence contains a polyhistidine tag to enable detection using western blot and protein purification using affinity chromatography. Expression of another MICOS subunit was also performed, but the experiments were not successful and were abandoned after initial attempts. The protein rMic32 is therefore visible in some Figures with a band at 34 kDa. The recombinant proteins were expressed according to the methods in Material and Methods section 3.2 and resolved by SDS-PAGE and western blot analysis utilizing antibodies for recognition of the poly-histidine tag to visualize if the expressed protein in the soluble or insoluble fraction. From Figure 6, it can be clearly seen that rMic20 is predominantly in the insoluble fraction of the lysates. The recombinant protein rMic20 has a size of 20kDa, elongated by the poly-histidine tag to 22kDa, whereas rMic32 has a size of 32kDa and 34kDa with poly-histidine tag, respectively.

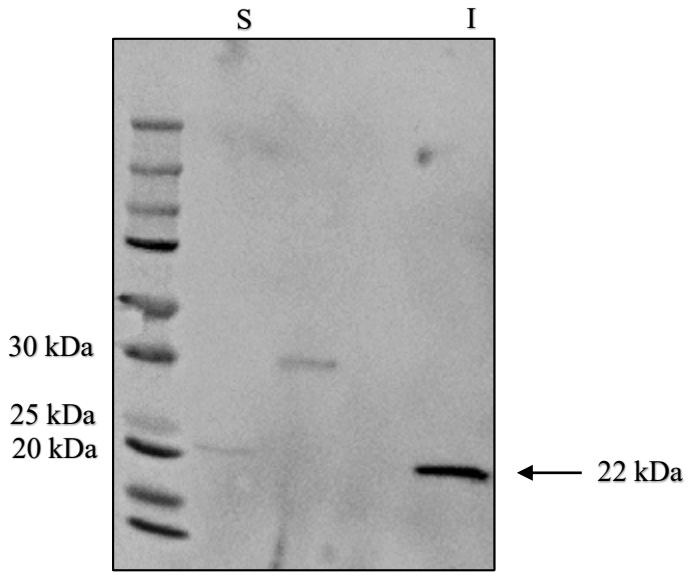

Figure 6: ***Expression and solubility test of rMic20 at 37°C for 1 hour:***
Soluble (S) and insoluble (I) fractions were resolved by SDS-PAGE and western blot analysis. 30µl of sample and 5µl of PageRuler unstained Protein Ladder as size standard was loaded. The bands corresponding to the proteins are marked with arrows.

The first attempt to increase the soluble fraction of the recombinant protein was made by lowering the temperature to 25°C and 14°C, following the same protocol for analysis of the protein described in Material and Methods according to section 3.2. Due to the decreased temperature, the rate of protein synthesis is decreased, and therefore the time after induction to the harvesting of the cell culture was increased to 14 hours at 25°C and 16 hours at 14°C. This is shown in Figure 7, as the intensity of the bands is decreased compared to the bands shown in Figure 1. Figure 7 also displays the increase of the soluble fraction, as in the expression at 14°C and 16 hours post-induction time, the soluble and insoluble fractions are almost equal.

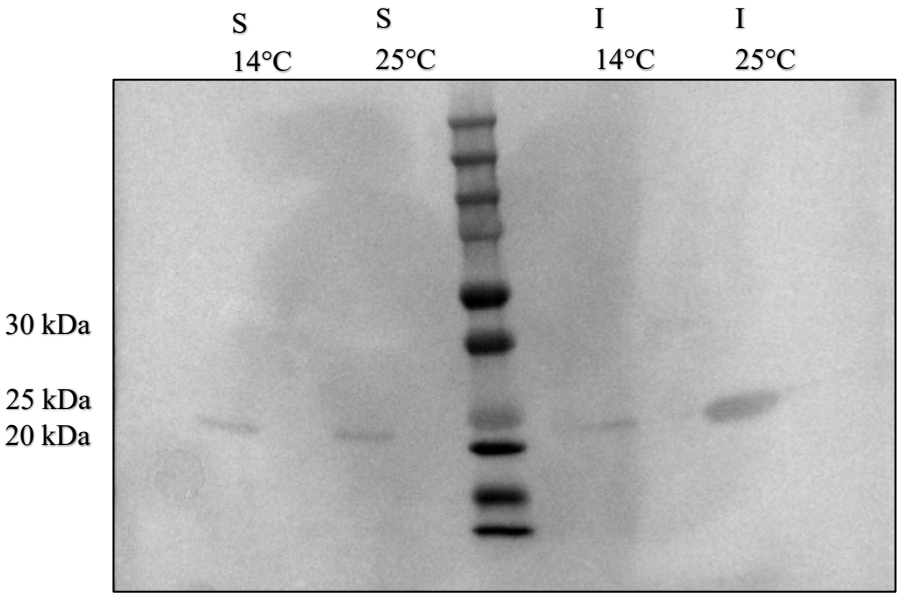

Figure 7: ***Expression and solubility test of rMic20 at 14°C for 16 hours and 25°C for 14 hours.*** *Soluble (S) and insoluble (I) fractions were resolved by SDS-PAGE and western blot analysis.* 30µl of sample and 5µl of PageRuler unstained Protein Ladder as size standard was loaded*. The band corresponding to the protein is marked with an arrow. An improvement of the condition can be observed in this Figure.*

The last solubility test of the recombinant protein was performed at 20°C, following the same protocol as described in Material and Methods according to section 3.2. In Figure 8, it is shown that the expression and purification yielded a slightly larger amount of soluble fraction, and it

was decided that the amount of soluble protein is sufficient to start the purification of the protein.

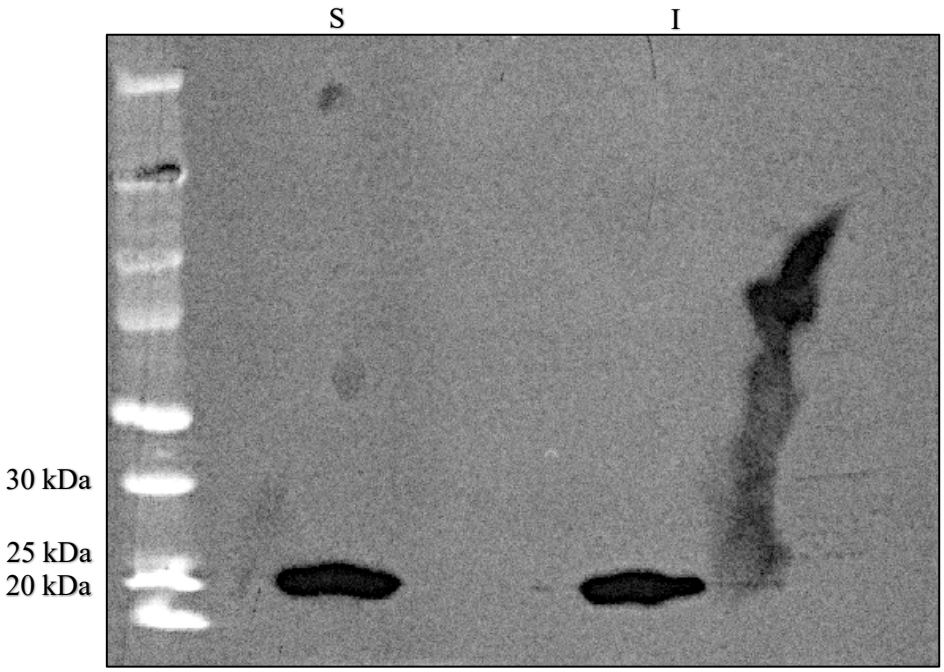

Figure 8: ***Expression and solubility test of rMic20 at 20°C for 14 hours.*** *The spot displayed in this Figure is an artefact that does not affect interpretation. Soluble (S) and insoluble (I) fractions were resolved using SDS-PAGE and western blot analysis. 30µl of sample and 5µl of PageRuler unstained Protein Ladder as size standard was loaded.*

4.2 Affinity chromatography

The recombinant protein was purified by performing affinity chromatography using Ni-NTA beads and a protocol according to section 3.3.1 resolved by SDS-PAGE according to section 3.2.3 and Coomassie blue staining according to section 3.3.2. In Figure 9, the band corresponding to rMic20 at 22kDa can be clearly identified in the elution fractions, and the protein concentration of elution 2 (E2) was determined with a NanoDrop™ 1000 Spectrophotometer (Thermo Scientific) and yielded a concentration of 2.9 mg/mL.

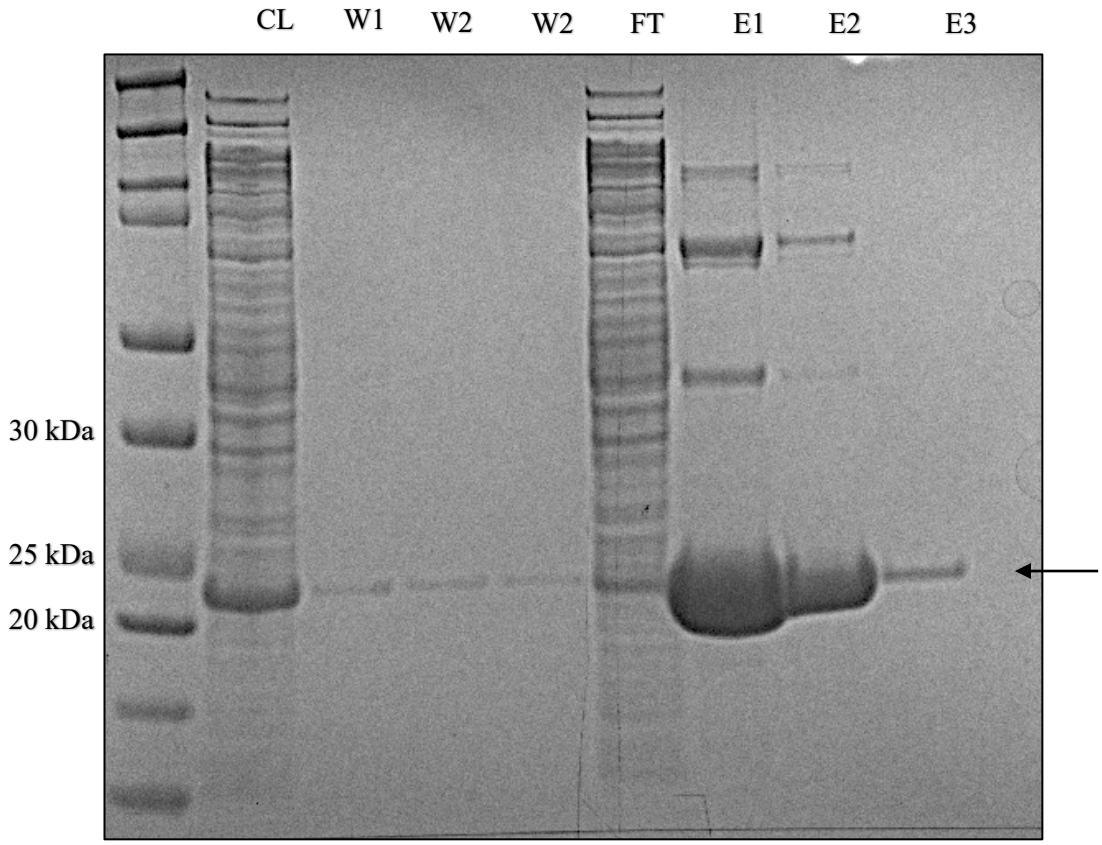

Figure 9: ***SDS-PAGE gel resolving purified proteins after affinity chromatography using Ni-NTA beads****. 30µl of sample and 5µl of PageRuler unstained Protein Ladder as size standard was loaded. CL = Cell Lysate; FT = Flow-through; W1-3 = washing fractions; E1-3 = Elution fractions. Visualization of the gel was performed using Coomassie Blue staining. The band corresponding to the recombinant protein is marked with an arrow.*

4.3 Cleavage of the poly-histidine tag of the recombinant protein

To address the redox potential of rMic20 and eliminate possible interaction of the poly-histidine tag, the tag was removed using AcTEV™ Protease (Invitrogen) according to section 3.3.3, followed by affinity chromatography. For confirmation of the cleavage, purified rMic20 after the usage of the AcTEV™ Protease Kit as well as a purified sample and rMic20 before poly-histidine tag cleavage as a control, were resolved with SDS-PAGE analysis and coomassie blue staining. As shown in Figure 10, the poly-histidine tag was successfully removed, indicated by the loss of 2 kDa. The protein concentration after the cleavage was determined to be 1.52 mg/mL with a NanoDrop™ 1000 Spectrophotometer (Thermo Scientific).

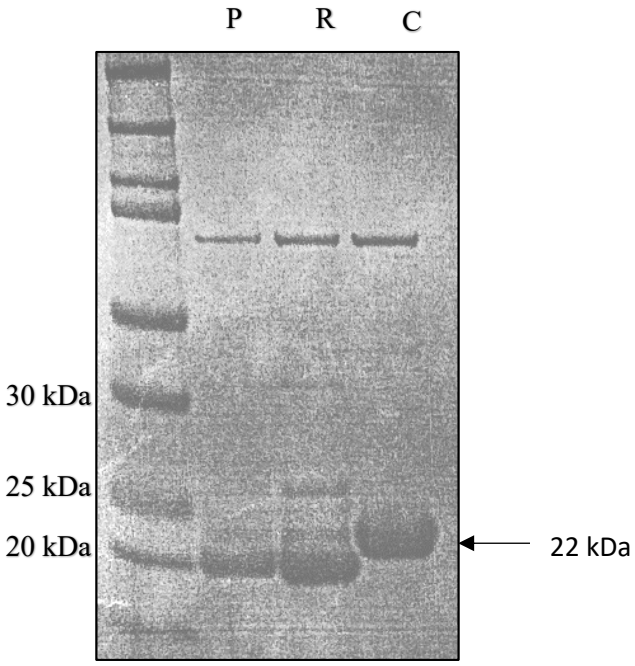

Figure 10: ***Confirmation of the histidine-tag cleavage resolved by SDS-PAGE and coomassie blue staining.*** *10µl of sample and 5µl of PageRuler unstained Protein Ladder as size standard was loaded. P = poly-histidine tag cleaved and purified by affinity chromatography; R = poly-histidine tag cleaved; C = rMic20 with poly-histidine tag. The band corresponding to the tagged recombinant protein is marked with an arrow.*

4.4 Assessing the redox potential of rMic20

Fluorescence spectroscopy was used to assess the redox potential of rMic20. For this purpose, an emission scan was performed to determine the wavelength of the largest difference of the oxidized and the reduced protein, making use of the fluorescence intensity difference between reduced and oxidized recombinant protein. The scan was performed according to section 3.4.1, and concentrations of 0.1 mM GSSG and 0.1 mM GSSG and ether 10 or 20 mM GSH were used. As shown in Figure 11, the largest difference in fluorescence can be observed at a wavelength of 333 nm, with the oxidized protein at a concentration of 0.1 mM GSSG and the fully reduced protein at 20 mM GSH.

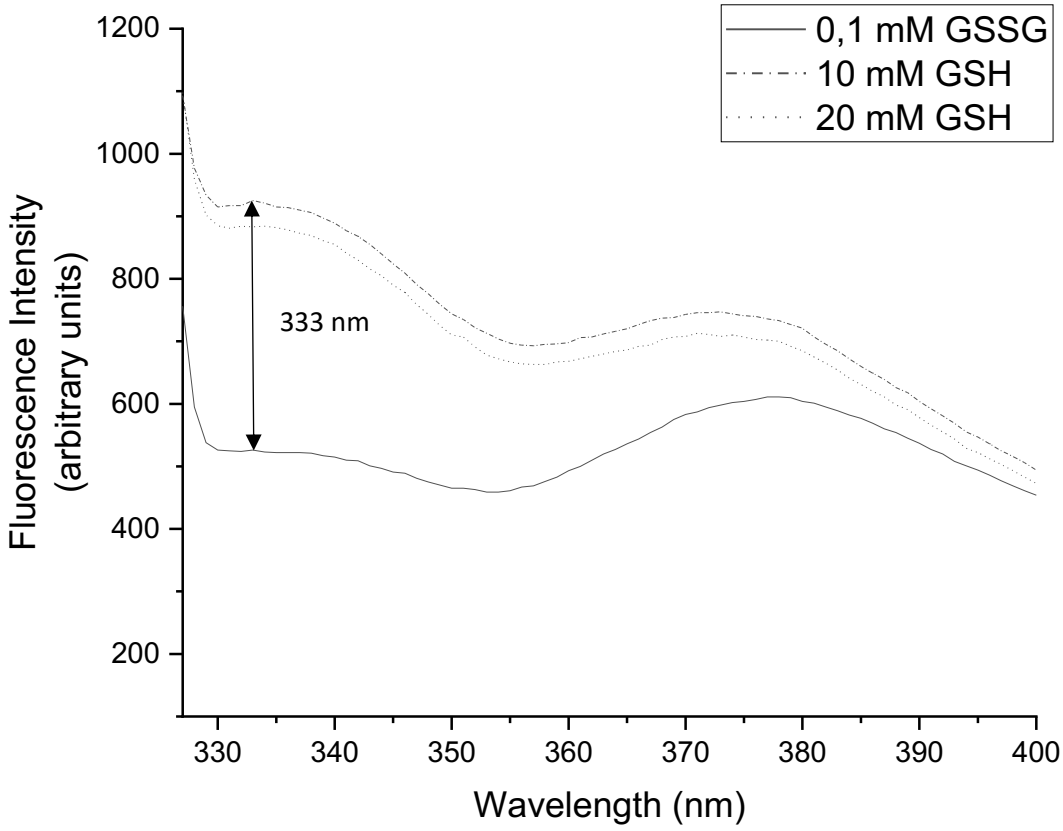

Figure 11: ***Fluorescence emission spectra of 5 µM rMic20 recorded of the reduced (50 mM phosphate buffer, pH 7.0 and 0.1 mM GSSG; dotted line) and the oxidized (50 mM phosphate buffer, pH 7.0 and 0.1 mM GSSG and 20 mM GSH; solid line)*** *The Figure shows a plot of the measured fluorescence intensity against the used excitation wavelength. 5 µM recombinant protein with either 0.1 mM GSSG, 0.1 mM GSSG and 10 mM GSH or 0.1 mM GSSG and 20 mM GSH, after excitation at 280 nm. The largest difference in fluorescence intensity is marked with an arrow at a wavelength of 333 nm.*

Using the determined wavelength of emission of 333 nm with the highest difference in fluorescence intensity between the oxidized and reduced recombinant protein, a fluorescence intensity scan was performed at an excitation of 280 nm. The relative amount of reduced protein was then determined using Equation 2 and plotted against the $[GSH]^2/[GSSG]$ ratio. Figure 12 shows the characteristic sigmoidal curve.

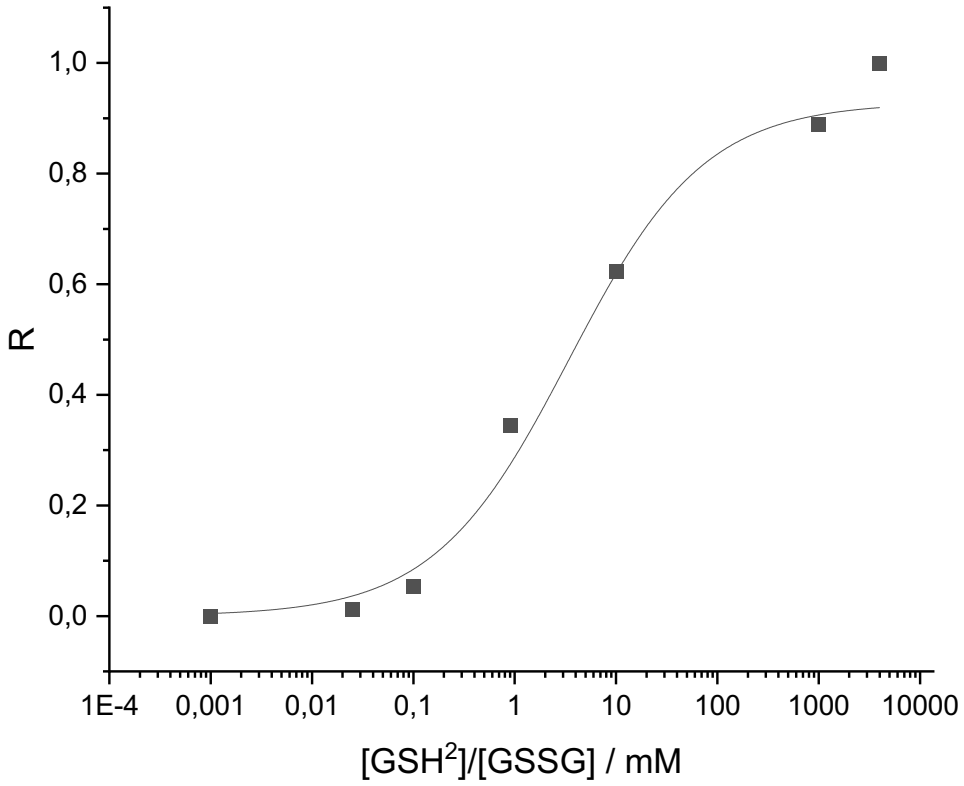

Figure 12: ***Plot of the [GSH]²/[GSSG] ratio against the relative amount of reduced protein.*** *The Figure shows a plot of the relative amount of reduced protein (R) against the [GSH]²/[GSSG] ratio. 5 µM recombinant protein with 0.1 mM GSSG and GSH in a range of 0.1M to 20 M. After excitation at 280 nm, the emission at wavelength 333 nm was recorded, and the R-value was calculated using Eq. 2.*

By linear transformation of the data obtained from Figure 12 using Equation 3, K_{eq} is equal to the negative intercept of the function (y = kx + d) and was determined to be $1{,}742 \times 10^{-2}$ M (Figure 13.). Using the Inserting in the Nernst Equation (Eq. 5) at pH 7.0, 298.15 K and using the standard potential of glutathione of -0,240 V (Müller, 2019), the standard redox potential E_0 of TbMic20 was determined to be -187,97 mV.

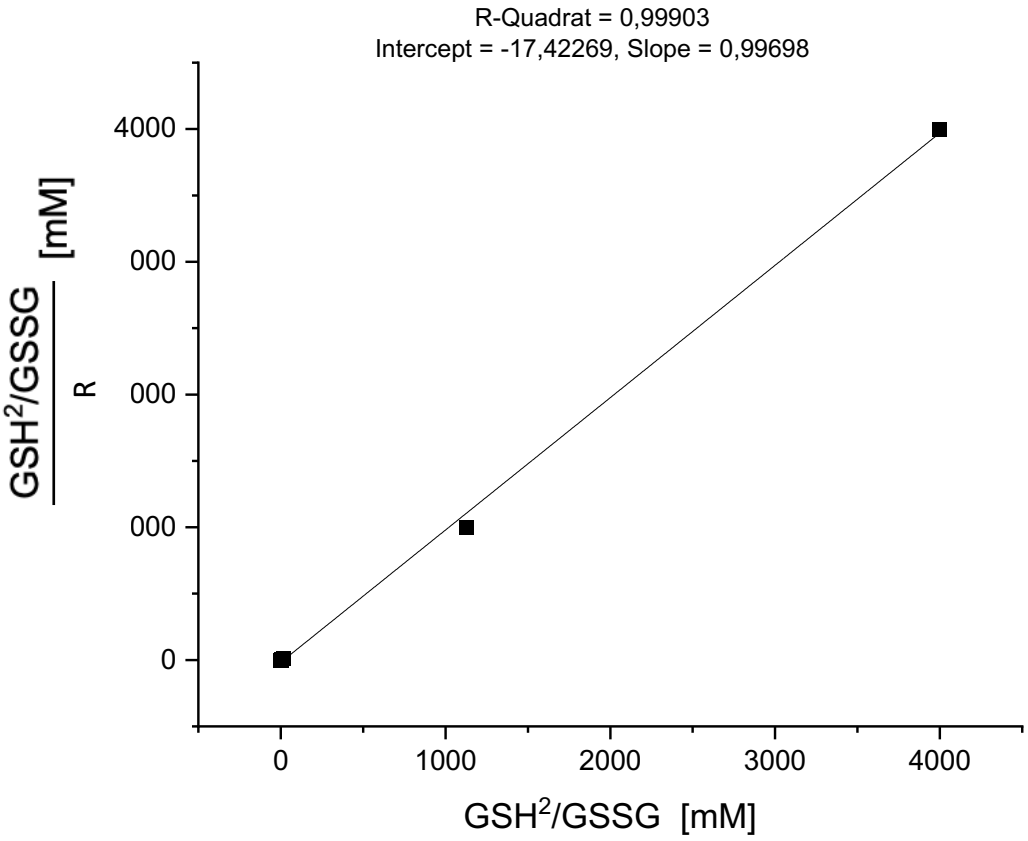

Figure 13: ***Linear transformation using Equation 2 and the data of Figure 1 to estimate K_{eq} by linear regression analysis.*** *The theoretical lines are obtained by linear regression of the data, where the negative intercept on the horizontal axis equals K_{eq}. The estimated value for K_{eq} is $1{,}742 \times 10^{-2}$ M.*

4.5 Site-directed mutagenesis

To change the redox-active CIPC motif of the recombinant protein, site-directed mutagenesis was performed.

The plasmid DNA of the cell construct containing the sequence of rMic20 was therefore extracted using a DNA purification kit (GeneAll®Hybrid-Q™ Plasmid Rapidprep). The length of the plasmid with the inserted gene of TbMic20 is 5869 bp long. By gel electrophoresis (Figure 14.), it was verified that the plasmid was successfully extracted and purified.

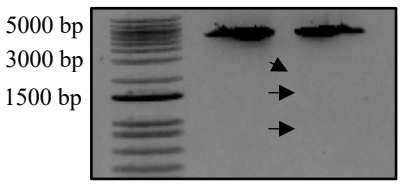

Figure 14: ***Verification of the plasmid extraction by gel electrophoresis.***

The site-directed mutagenesis was then performed using a BioRad C1000^{TM} Thermal cycler according to section 3.5.3. A negative control containing only the reaction mixture without plasmid DNA was also added to the Thermal cycler, to detect possible contamination with foreign DNA.

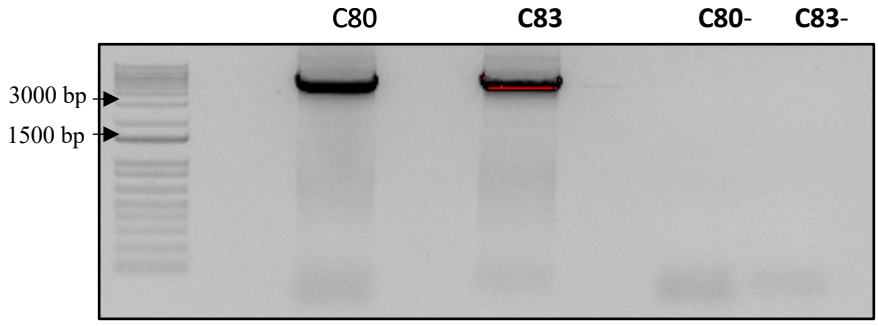

Figure 15: ***Verification of the site-directed mutagenesis products using gel electrophoresis.*** *25 µL of sample + 5 µL of LD were loaded on the gel.*

The success of the site-directed mutagenesis was proven by lab technician RNDr. Heller Jiri. The isolated DNA was sent to Eurofins Scientific for sequence analysis and the sequence data obtained is listed in Table 17.

Table 17: ***Sequence of rMic20 and sequence data of the created C80 and C83 mutants obtained from Eurofins Scientific.*** *CIPC motif and exchanged amino acid in bold.*

Name	***Length***	***Sequence***
rMic20	167 aa 501 bp	MTQNIIRRIFGNRELPENLSGSEYERYMQENFPKWIDEFEKGGFLEAT KLPAIKSERDFLSKLIEHKDEIMVVKYWKHG**CIPC**LSLAEMYKQVSE QCKKENRRIAWYSVNTKDVSARSLVDYQLVNGTPTVQTFSRMKQV GKEIRAISAEELMRELSREAALNTES
C80	167 aa 501 bp	MTQNIIRRIFGNRELPENLSGSEYERYMQENFPKWIDEFEKGGFLEAT KLPAIKSERDFLSKLIEHKDEIMVVKYWKHG**SIPC**LSLAEMYKQVSE QCKKENRRIAWYSVNTKDVSARSLVDYQLVNGTPTVQTFSRMKQV GKEIRAISAEELMRELSREAALNTES
C83	167 aa 501 bp	MTQNIIRRIFGNRELPENLSGSEYERYMQENFPKWIDEFEKGGFLEAT KLPAIKSERDFLSKLIEHKDEIMVVKYWKHG**CIPS**LSLAEMYKQVSE QCKKENRRIAWYSVNTKDVSARSLVDYQLVNGTPTVQTFSRMKQV GKEIRAISAEELMRELSLREAALNTES

5. Discussion

To get in vitro data for TbMICOS subunit TbMic20 as the functional analogue of the central MIA enzyme Mia40, the standard redox potential of the protein was determined. For this purpose, a pSKB-3 plasmid containing a polyhistidine-tagged TbMic20 transformed to *Escherichia Coli* BL21-strain was used for the expression of the recombinant protein and the procedure was optimized for an increase in solubility. Proteins are often insoluble due to aggregation and precipitation, and several ways can be used to increase solubility. The decrease of temperature or the decrease of the IPTG concentration to reduce the protein synthesis to prevent aggregation or precipitation is widely used. It was found that the decrease of the expression temperature to 20°C and elongation of the time to 14 hours resulted in a sufficient amount of the soluble fraction of the recombinant protein (Figure 8).

By affinity chromatography using Novex™ Ni-NTA Agarose (Invitrogen™), the recombinant protein was successfully purified (Figure 9). To remove possible interaction of the his-tag in the following experiments, the his-tag was removed using AcTEV™ Protease (Invitrogen), and a modified procedure (Figure 10) and the His-tag residues were removed subsequently by repeating affinity chromatography. Novex™ Ni-NTA Agarose (Invitrogen™) bind specifically to a poly-histidine tag and therefore enable the purification of the recombinant protein in both steps.

To determine the standard redox potential of the recombinant protein, various fluorescence measurements were performed (Figure 11-12). The value for E_0 was determined at pH 7.0 to be -188 mV (Figure 13). The standard redox potentials of the thioredoxin family of thiol-disulfide oxidoreductases range from -124 mV to -270 mV, which the determined value for TbMic20 falls in (Åslund et al., 1997). In comparison, the standard redox potential of Mia40 lies at -200 ± 5mV. Oxidation of substrates with more reducing potential is favoured upon the standard redox potential of the CIPC motif (-188 mV) of TbMic20 (Banci et al., 2009). Therefore, showing more evidence that TbMic20 might be the functional analogue of Mia40 in trypanosomes.

Site-directed mutagenesis was performed to create mutants, which express the recombinant protein without the characteristic CIPC motif. Figure 15 shows that the thermo-cycler program was successful. Unfortunately, the following DNA isolation failed for unknown reasons, which resulted in improper results of the restriction digestion. Due to the end of my stay in České Budějovice, I was not able to repeat these experiments and confirm the success of the mutagenesis myself. However, RNDr. Jiri Heller repeated the DNA isolation and the following experiments and was able to successfully confirm the site-directed mutagenesis. Through the creation of the mutant proteins, it is possible to compare its structure and functions to the wild-type protein and thereby enables further examination of the biochemical properties of TbMic20.

6. Conclusion

In the presented work, we were able to assess the redox potential of the rProtein Mic20 of *Trypanosome brucei*.

Through use of various molecular biological techniques, it was possible to express rMic20 in *E. coli* under soluble condition to further examine the activity of the protein. The protein then was successfully purified using affinity chromatography.

Using fluorescence measurements using GSSG and GSH to reduce and oxidize rMic20, we were able to assess the redox potential of the protein at -188 mV, which lies in the range of other thioredoxin-like proteins (Åslund et al., 1997).

PCR based site-directed mutagenesis was successfully used to exchange the cysteine of the characteristic CIPC motif with serine and it was possible to transform the mutant DNA into *E. coli* cells to express the mutant protein. RNDr. Jiri Heller was able to confirm the result by sequencing of the mutant DNA isolated from the prepared *E. coli* cell culture.

7. References

Allen, J. W. A., Ferguson, S. J., & Ginger, M. L. (2008). Distinctive biochemistry in the trypanosome mitochondrial intermembrane space suggests a model for stepwise evolution of the MIA pathway for import of cysteine-rich proteins. *FEBS Letters*, *582*(19), 2817–2825. https://doi.org/10.1016/j.febslet.2008.07.015

Åslund, F., Berndt, K. D., & Holmgren, A. (1997). Redox Potentials of Glutaredoxins and Other Thiol-Disulfide Oxidoreductases of the Thioredoxin Superfamily Determined by Direct Protein-Protein Redox Equilibria. *Journal of Biological Chemistry*, *272*(49). https://doi.org/10.1074/jbc.272.49.30780

Banci, L., Bertini, I., Cefaro, C., Ciofi-Baffoni, S., Gallo, A., Martinelli, M., Sideris, D. P., Katrakili, N., & Tokatlidis, K. (2009). MIA40 is an oxidoreductase that catalyzes oxidative protein folding in mitochondria. *Nature Structural & Molecular Biology*, *16*(2). https://doi.org/10.1038/nsmb.1553

Barbot, M., Jans, D. C., Schulz, C., Denkert, N., Kroppen, B., Hoppert, M., Jakobs, S., & Meinecke, M. (2015). Mic10 Oligomerizes to Bend Mitochondrial Inner Membranes at Cristae Junctions. *Cell Metabolism*, *21*(5). https://doi.org/10.1016/j.cmet.2015.04.006

Barbot, M., & Meinecke, M. (2016). Reconstitutions of mitochondrial inner membrane remodeling. *Journal of Structural Biology*, *196*(1). https://doi.org/10.1016/j.jsb.2016.07.014

Bohnert, M., Zerbes, R. M., Davies, K. M., Mühleip, A. W., Rampelt, H., Horvath, S. E., Boenke, T., Kram, A., Perschil, I., Veenhuis, M., Kühlbrandt, W., van der Klei, I. J., Pfanner, N., & van der Laan, M. (2015). Central Role of Mic10 in the Mitochondrial Contact Site and Cristae Organizing System. *Cell Metabolism*, *21*(5), 747–755. https://doi.org/10.1016/j.cmet.2015.04.007

Böttinger, L., Gornicka, A., Czerwik, T., Bragoszewski, P., Loniewska-Lwowska, A., Schulze-Specking, A., Truscott, K. N., Guiard, B., Milenkovic, D., & Chacinska, A. (2012). In vivo evidence for cooperation of Mia40 and Erv1 in the oxidation of mitochondrial proteins. *Molecular Biology of the Cell*, *23*(20). https://doi.org/10.1091/mbc.e12-05-0358

Brun, R., Blum, J., Chappuis, F., & Burri, C. (2010). Human African trypanosomiasis. *The Lancet*, *375*(9709). https://doi.org/10.1016/S0140-6736(09)60829-1

Chacinska, A., Pfannschmidt, S., Wiedemann, N., Kozjak, V., Sanjuán Szklarz, L. K., Schulze-Specking, A., Truscott, K. N., Guiard, B., Meisinger, C., & Pfanner, N. (2004). Essential role of Mia40 in import and assembly of mitochondrial intermembrane space proteins. *The EMBO Journal*, *23*(19). https://doi.org/10.1038/sj.emboj.7600389

Chatzi, A., Sideris, D. P., Katrakili, N., Pozidis, C., & Tokatlidis, K. (2013). Biogenesis of yeast Mia40—Uncoupling folding from import and atypical recognition features. *FEBS Journal*, *280*(20). https://doi.org/10.1111/febs.12482

Davies, K. M., Strauss, M., Daum, B., Kief, J. H., Osiewacz, H. D., Rycovska, A., Zickermann, V., & Kühlbrandt, W. (2011). Macromolecular organization of ATP synthase

and complex I in whole mitochondria. *Proceedings of the National Academy of Sciences*, *108*(34), 14121–14126. https://doi.org/10.1073/pnas.1103621108

Dolezal, P., Likic, V., Tachezy, J., & Lithgow, T. (2006). Evolution of the Molecular Machines for Protein Import into Mitochondria. *Science*, *313*(5785), 314–318. https://doi.org/10.1126/science.1127895

Edwards, R., Gerlich, S., & Tokatlidis, K. (2020). The biogenesis of mitochondrial intermembrane space proteins. *Biological Chemistry*, *401*(6–7), 737–747. https://doi.org/10.1515/hsz-2020-0114

Friedman, J. R., Mourier, A., Yamada, J., McCaffery, J. M., & Nunnari, J. (2015). MICOS coordinates with respiratory complexes and lipids to establish mitochondrial inner membrane architecture. *eLife*, *4*, e07739. https://doi.org/10.7554/eLife.07739

Gilkerson, R. W., Selker, J. M. L., & Capaldi, R. A. (2003). The cristal membrane of mitochondria is the principal site of oxidative phosphorylation. *FEBS Letters*, *546*(2), 355–358. https://doi.org/10.1016/S0014-5793(03)00633-1

Guarani, V., McNeill, E. M., Paulo, J. A., Huttlin, E. L., Fröhlich, F., Gygi, S. P., Van Vactor, D., & Harper, J. W. (2015). QIL1 is a novel mitochondrial protein required for MICOS complex stability and cristae morphology. *eLife*, *4*, e06265. https://doi.org/10.7554/eLife.06265

Haindrich, A. C., Boudová, M., Vancová, M., Diaz, P. P., Horáková, E., & Lukeš, J. (2017). The intermembrane space protein Erv1 of Trypanosoma brucei is essential for mitochondrial Fe-S cluster assembly and operates alone. *Molecular and Biochemical Parasitology*, *214*, 47–51. https://doi.org/10.1016/j.molbiopara.2017.03.009

Harner, M., Körner, C., Walther, D., Mokranjac, D., Kaesmacher, J., Welsch, U., Griffith, J., Mann, M., Reggiori, F., & Neupert, W. (2011). The mitochondrial contact site complex, a determinant of mitochondrial architecture: Molecular architecture of mitochondria. *The EMBO Journal*, *30*(21), 4356–4370. https://doi.org/10.1038/emboj.2011.379

Haugstetter, J., Blicher, T., & Ellgaard, L. (2005). Identification and Characterization of a Novel Thioredoxin-related Transmembrane Protein of the Endoplasmic Reticulum. *Journal of Biological Chemistry*, *280*(9). https://doi.org/10.1074/jbc.M413924200

Hawkins, H. C., de Nardi, M., & Freedman, R. B. (1991). Redox properties and cross-linking of the dithiol/disulphide active sites of mammalian protein disulphide-isomerase. *Biochemical Journal*, *275*(2). https://doi.org/10.1042/bj2750341

Höög, J. L., Gluenz, E., Vaughan, S., & Gull, K. (2010). *Ultrastructural Investigation Methods for Trypanosoma brucei*. https://doi.org/10.1016/S0091-679X(10)96008-1

Huynen, M. A., Mühlmeister, M., Gotthardt, K., Guerrero-Castillo, S., & Brandt, U. (2016). Evolution and structural organization of the mitochondrial contact site (MICOS) complex and the mitochondrial intermembrane space bridging (MIB) complex. *Biochimica et Biophysica Acta (BBA) - Molecular Cell Research*, *1863*(1). https://doi.org/10.1016/j.bbamcr.2015.10.009

Kaurov, I., Vancová, M., Schimanski, B., Cadena, L. R., Heller, J., Bílý, T., Potěšil, D., Eichenberger, C., Bruce, H., Oeljeklaus, S., Warscheid, B., Zdráhal, Z., Schneider, A., Lukeš, J., & Hashimi, H. (2018). The Diverged Trypanosome MICOS Complex as a Hub for Mitochondrial Cristae Shaping and Protein Import. *Current Biology*, *28*(21). https://doi.org/10.1016/j.cub.2018.09.008

Koch, J. R., & Schmid, F. X. (2014). Mia40 Combines Thiol Oxidase and Disulfide Isomerase Activity to Efficiently Catalyze Oxidative Folding in Mitochondria. *Journal of Molecular Biology*, *426*(24). https://doi.org/10.1016/j.jmb.2014.10.022

Loferer, H., Wunderlich, M., Hennecke, H., & Glockshuber, R. (1995). A Bacterial Thioredoxin-like Protein That Is Exposed to the Periplasm Has Redox Properties Comparable with Those of Cytoplasmic Thioredoxins. *Journal of Biological Chemistry*, *270*(44). https://doi.org/10.1074/jbc.270.44.26178

Matthews, K. R. (2005). The developmental cell biology of Trypanosoma brucei. *Journal of Cell Science*, *118*(2). https://doi.org/10.1242/jcs.01649

Matthews, K. R., Ellis, J. R., & Paterou, A. (2004). Molecular regulation of the life cycle of African trypanosomes. *Trends in Parasitology*, *20*(1). https://doi.org/10.1016/j.pt.2003.10.016

Milenkovic, D., Gabriel, K., Guiard, B., Schulze-Specking, A., Pfanner, N., & Chacinska, A. (2007). Biogenesis of the Essential Tim9–Tim10 Chaperone Complex of Mitochondria: SITE-SPECIFIC RECOGNITION OF CYSTEINE RESIDUES BY THE INTERMEMBRANE SPACE RECEPTOR Mia40 *. *Journal of Biological Chemistry*, *282*(31), 22472–22480. https://doi.org/10.1074/jbc.M703294200

Mordas, A., & Tokatlidis, K. (2015). The MIA Pathway: A Key Regulator of Mitochondrial Oxidative Protein Folding and Biogenesis. *Accounts of Chemical Research*, *48*(8). https://doi.org/10.1021/acs.accounts.5b00150

Müller, F. (2019). *Chemistry and biochemistry of flavoenzymes. Volume III Volume III*. https://search.ebscohost.com/login.aspx?direct=true&scope=site&db=nlebk&db=nlabk&AN=2206709

Muñoz-Gómez, S. A., Slamovits, C. H., Dacks, J. B., Baier, K. A., Spencer, K. D., & Wideman, J. G. (2015). Ancient Homology of the Mitochondrial Contact Site and Cristae Organizing System Points to an Endosymbiotic Origin of Mitochondrial Cristae. *Current Biology*, *25*(11). https://doi.org/10.1016/j.cub.2015.04.006

Narayan, M., Welker, E., Wedemeyer, W. J., & Scheraga, H. A. (2000). Oxidative Folding of Proteins. *Accounts of Chemical Research*, *33*(11). https://doi.org/10.1021/ar000063m

Pánek, T., Eliáš, M., Vancová, M., Lukeš, J., & Hashimi, H. (2020). Returning to the Fold for Lessons in Mitochondrial Crista Diversity and Evolution. *Current Biology*, *30*(10). https://doi.org/10.1016/j.cub.2020.02.053

Roger, A. J., Muñoz-Gómez, S. A., & Kamikawa, R. (2017). The Origin and Diversification of Mitochondria. *Current Biology*, *27*(21), R1177–R1192. https://doi.org/10.1016/j.cub.2017.09.015

Simpson, A. G. B., Lukeš, J., & Roger, A. J. (2002). The Evolutionary History of Kinetoplastids and Their Kinetoplasts. *Molecular Biology and Evolution*, *19*(12). https://doi.org/10.1093/oxfordjournals.molbev.a004032

Stojanovski, D., Bragoszewski, P., & Chacinska, A. (2012). The MIA pathway: A tight bond between protein transport and oxidative folding in mitochondria. *Biochimica et Biophysica Acta (BBA) - Molecular Cell Research*, *1823*(7). https://doi.org/10.1016/j.bbamcr.2012.04.014

Stuart, K., Brun, R., Croft, S., Fairlamb, A., Gürtler, R. E., McKerrow, J., Reed, S., & Tarleton, R. (2008). Kinetoplastids: Related protozoan pathogens, different diseases. *Journal of Clinical Investigation*, *118*(4). https://doi.org/10.1172/JCI33945

Wideman, J. G., & Muñoz-Gómez, S. A. (2018). Cell Biology: Functional Conservation, Structural Divergence, and Surprising Convergence in the MICOS Complex of Trypanosomes. *Current Biology*, *28*(21). https://doi.org/10.1016/j.cub.2018.09.057